Proceedings of the ASME 28th International Conference on Ocean, Offshore and Arctic Engineering
OMAE2009
May 31 – June 5, 2009, Honolulu, Hawaii

OMAE2009-80050

THE INFLUENCE OF FOUNDATION MODELING ASSUMPTIONS ON LONG-TERM LOAD PREDICTION FOR OFFSHORE WIND TURBINES

Erica Bush
University of Texas at Austin
Austin, TX, USA

Lance Manuel
University of Texas at Austin
Austin, TX, USA

ABSTRACT

The objective of this study is to investigate the effect of alternative monopile foundation models for shallow-water offshore wind turbines on extreme loads associated with 20-year return periods. Foundation models with tower base fixed at the mudline, with apparent fixity points below the mudline, with coupled transverse and lateral springs at the mudline, and with distributed springs over the entire penetration depth of the monopile are compared. We employ a utility-scale 5 MW offshore wind turbine model with a 90-meter hub height in stochastic simulations; the turbine is sited in 20 meters of water. Selected 20-year wind speed and wave height combinations are employed as we study comparative response statistics, power spectra, and probability distributions of extreme loads for the fixed-base and the three different flexible foundation models. A discussion on the varying dynamics, on short-term response statistics, and on extrapolated long-term loads from limited simulation is presented. Sea states involving wind speeds close to the turbine's rated wind speed are found to control 20-year loads, and the flexible foundation models are found to experience higher extreme loads than the fixed-based case. Overall, the three flexible foundation models appear to yield similar long-term loads based on an Inverse FORM (First-Order Reliability Method) approach for the selected turbine and soil profile used in this study.

INTRODUCTION

Characteristic or nominal loads for the design of wind turbines in ultimate limit states are generally established by employing time-domain aeroelastic response simulations. The accuracy of the derived loads depends on the number of simulations and on how realistically the models used to represent the turbine, support structure, and foundation describe the true structural behavior. One potential shortcoming in modeling offshore wind turbine foundations relates to their flexibility. A single pile (often referred to as a monopile) is a very common type of foundation used for offshore wind turbines; the turbine support structure connects to such a pile foundation that extends some depth below the mudline. We present four different foundation models. The fixed-base (FB) model is the simplest of the four and assumes a perfectly rigid connection of the turbine's support structure with the seabed. This model does not consider the soil profile at the turbine site, and it does not allow for lateral or rocking motion at the mudline. The other three foundation models are "flexible" by contrast with the FB model, and how they are defined depends on the soil profile at the turbine site. The apparent fixity (AF) model assumes that the turbine tower is fixed (as a cantilever, without surrounding soil) at a depth below the original mudline; this fixity depth is determined such that it produces a specified lateral displacement and rotation at the mudline that matches that of the pile embedded in the true soil profile. The coupled springs (CS) model replaces the soil with coupled rotational and translational springs at the mudline, whose properties need to be determined. The distributed springs (DS) model is defined over the true length of the monopile foundation; it involves replacement of layers of the soil with linear elastic springs, whose properties again need to be determined. Figure 1 illustrates the three flexible foundation models together with the fixed-base model. These models are based largely on the work of Passon [1]; they are also summarized in a study by Jonkman et al [2]. We consider each of the four foundation models in critical environmental conditions believed to control long-term tower loads, in stochastic simulations of a 5 MW offshore wind turbine sited in 20 meters of water. Extreme load statistics, specifically for the fore-aft tower bending moment at the mudline, are compared for the four foundation models.

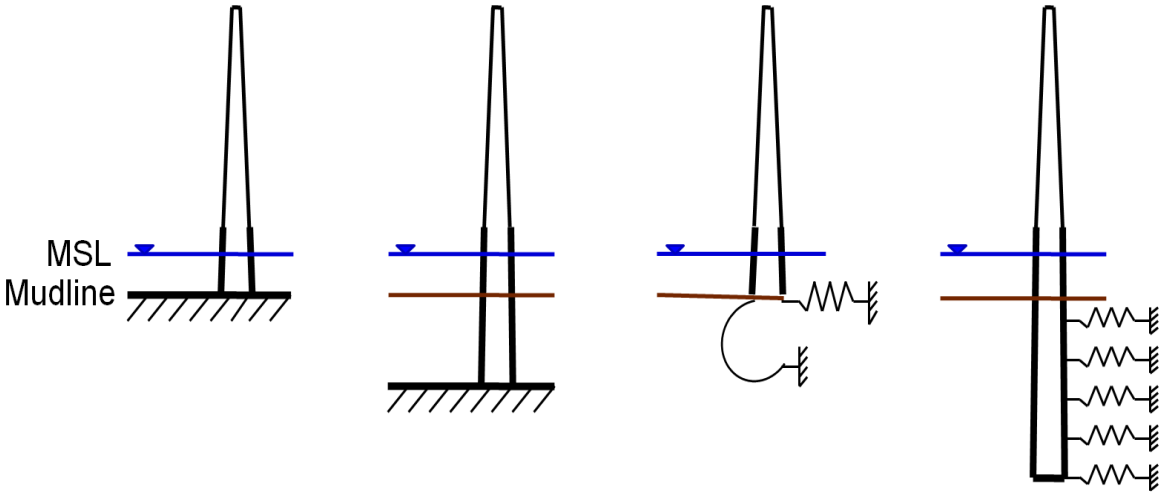

Figure 1: Alternative foundation models analyzed in this study.

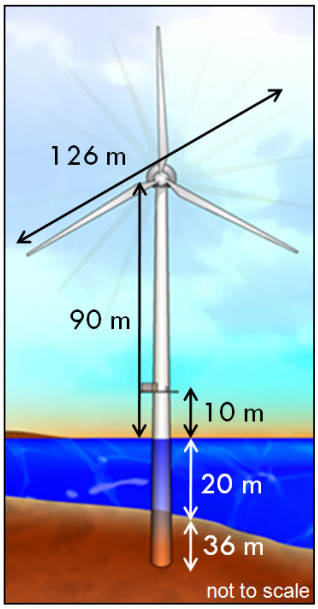

Figure 2: Dimensioned wind turbine, support structure, and foundation.

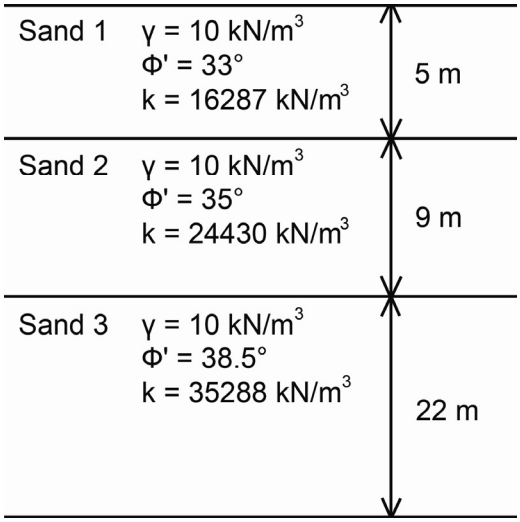

Figure 3: Soil profile at the wind turbine site.

MODEL OF THE OFFSHORE WIND TURBINE

A 5 MW wind turbine model [3], developed at the National Renewable Energy Laboratory (NREL), that is representative of utility-scale offshore wind turbines being manufactured today, is the subject of our study. The turbine is a variable-speed, collective pitch-controlled machine with a maximum rotor speed of 12.1 rpm; its rated wind speed is 11.5 m/s. It has a hub 90 meters above the mean sea level and a rotor diameter of 126 meters; it is sited in 20 meters of water. The wind turbine's tower, support structure, and monopile foundation are modeled as a single continuous cylindrical tube with varying diameter and wall thickness. The density of steel of which the tower is constructed is taken to be 8,500 kg/m^3, and the modulus of elasticity is taken to be 2.1×10^5 MN/m^2. The tower, attached to the support structure, tapers linearly upward—at the top, the tower has an outer diameter of 3.87 m and a wall thickness of 1.9 cm; at 10 m above the mean sea level, the tower has an outer diameter of 6 m and a wall thickness of 2.7 cm. The monopile support structure for the tower starts 10 m above the

mean sea level; over its length, it has a constant outer diameter of 6 m and a constant wall thickness of 6 cm. At the mudline, this support structure attaches to the monopile foundation of the same dimensions; the foundation is embedded 36 m into the seabed. Figure 2 shows the wind turbine, support structure, and foundation with dimensions. The soil profile at the site under consideration is shown in Fig. 3; this is the same profile used by Passon [1]. In the figure, γ refers to the effective weight, Φ' refers to the angle of internal friction, and k refers to the initial modulus of the subgrade reaction.

TURBINE RESPONSE SIMULATIONS

We are interested in evaluating the influence of alternative foundation modeling assumptions on extreme wind turbine tower loads based on stochastic response simulations for selected wind-wave environmental conditions. The environmental contour method (referred to here as 2D Inverse FORM [4] because of the two environmental random variables, V and H_s, involved) is used to identify candidate sea states, all associated with a 20-year return period. From these sea states, a single one must be found that is then the controlling sea state for the characteristic tower load of the wind turbine. Table 1 lists two of the environmental contour (EC) sea states that were selected for the present study. Each sea state is represented by the hub-height ten-minute average wind speed, V, and the significant wave height, H_s. Note that the wave spectral peak period, T_p, is deterministically related to the significant wave height in specification of the JONSWAP spectrum for the waves [5]. Also, the Normal Turbulence Model (NTM) [6] is employed to relate the hub-height turbulence intensity to V.

Table 1: Two 20-year return period sea states considered in the wind turbine loads study.

V (m/s)	H_s (m)
12	6.2
22	9.0

Kaimal power spectra and exponential coherence functions are employed to describe the inflow turbulence random field over the rotor plane, which is simulated using the computer program, TurbSim [7]. For the hydrodynamic loading on the support structure, irregular long-crested waves are simulated using a JONSWAP spectrum [8]. Power spectra for the hub-height longitudinal wind speed and the sea surface elevation are shown in Fig. 4 for the two selected sea states. After obtaining time series of the inflow turbulence field using TurbSim, time-domain stochastic simulations of the turbine response are carried out using FAST [9], which employs a combined modal and multi-body dynamics formulation. It accounts for aerodynamic loads based on the inflow turbulence input; it also accounts for hydrodynamic loads by first simulating a random sea surface elevation process, and then applying appropriate wave kinematics and inertia and drag force computations using Morison's equation [5].

We are interested in comparing tower loads for the fixed-base (FB) model, the apparent fixity (AF) model, the coupled springs (CS) model, and the distributed springs (DS) model. For each sea state, a total of 150 ten-minute turbine response simulations are carried out with each of these four foundation models. The different flexible foundation models are discussed next.

FLEXIBLE FOUNDATION MODELS

A. Apparent Fixity Model

In the apparent fixity model, the true monopile foundation and the surrounding soil medium are replaced by a cantilevered cylinder that is fixed not at the original mudline but at a lower depth whose location is derived as a point of apparent fixity [1, 2]. The associated flexural rigidity of the fictitious pile is derived as well. The apparent fixity length (L) represents the depth below the mudline where a cantilevered monopile would have the same stiffness as the true pile-soil system. Given specified levels of fore-aft tower shear (F) and moment (M) at the mudline, lateral deflections and rotations of the pile at that same location are first determined using the known soil profile, penetration depth, and pile dimension/properties. This is typically carried out using a pile lateral load analysis program such as LPILE [10]. Within an LPILE analysis, p-y curves (lateral force-displacement relationships) are generated for the soil properties defined in Fig. 3. The p-y curves are based on guidelines provided by the American Petroleum Institute [11] for offshore platforms. Note that an axial force in the pile is also needed in order to account for secondary moments (so-called P-Δ effects) when the pile deflects laterally. However, the shear and moment are of greater importance since deformations are generally small leading to negligible secondary effects.

Since the nonlinear p-y curves yield different foundation stiffness values (and, thus, different apparent fixity lengths) depending on the applied shear and moment at the mudline, the F and M values selected for establishing the AF model are important. In our analyses, we employ representative mudline shear and moment values based on preliminary fixed-base (FB) simulations in the selected sea states. In order to represent mudline shear and moment pairs from an entire ten-minute simulation, all of the contemporaneous pairs from the simulation for the selected sea state were sorted into 25 bins that covered the entire range of F and M values experienced in the simulations. As many FB simulations were added to the 25 bins as necessary until the relative frequency of each F-M bins was reasonably stable. For the V = 12 m/s sea state and the V = 22 m/s sea state, a total of 13 and 8 FB simulations, respectively, were necessary. Next, LPILE was run for all the 25 F-M pairs representing midpoints of the selected bins, and the deflection and rotation of the pile at the mudline were determined.

Next, the apparent fixity length and flexural rigidity were calculated for all the 25 bins. The length of the equivalent cantilever that replaces the true soil-pile system is that which will produce the same rotation (θ) and lateral deflection (w) at its free end (the original mudline) under the shear (F) and moment (M) applied at the mudline. This is referred to as the apparent fixity length (L) and is derived along with the flexural rigidity (EI) of the cantilever using the following equation:

$$\begin{bmatrix} \frac{L^3}{3EI} & \frac{L^2}{2EI} \\ \frac{L^2}{2EI} & \frac{L}{EI} \end{bmatrix} \begin{Bmatrix} F \\ M \end{Bmatrix} = \begin{Bmatrix} w \\ \theta \end{Bmatrix} \quad (1)$$

The 25 L and EI values, each associated with one of the 25 F-M bins, were then weighted according to that bin's relative likelihood. This weighted average approach produced a single apparent fixity length and flexural rigidity value that could then be used for each AF simulation per sea state. These L and EI values for the two sea states are summarized in Table 2.

To model this fictitious cylinder in FAST, its length, flexural rigidity, and mass distribution are required. The length and flexural rigidity are determined as described by Eq. (1). The mass distribution (i.e., the mass per unit length) is taken to be the mass of the original 36-meter foundation divided by the apparent fixity length. This ensures that the total mass of the AF model is the same as that of the original structure.

Table 2: Apparent fixity length and flexural rigidity values for the monopile used in the AF model (for two sea states).

V (m/s)	L (m)	EI (MN-m^2)
12	16.21	1.09 x 10^6
22	16.77	1.06 x 10^6

B. Coupled Springs Model

The coupled springs (CS) model reduces soil behavior to the consideration of linear elastic translational and rotational springs at the mudline [1,2]; hence, there is no monopile section to include below that level. The spring constants are derived from the AF analysis; the CS model uses the same apparent fixity length and flexural rigidity values for the different sea states as in the AF model. Because the shear, moment, deflection, and rotation all occur at the mudline, the coefficient matrix of Eq. (1) represents the soil-pile flexibility at the mudline. Required spring stiffnesses for the CS model can be derived by rewriting Eq. (1) using a stiffness formulation as follows:

$$\begin{bmatrix} \frac{12EI}{L^3} & -\frac{6EI}{L^2} \\ -\frac{6EI}{L^2} & \frac{4EI}{L} \end{bmatrix} \begin{Bmatrix} w \\ \theta \end{Bmatrix} = \begin{Bmatrix} F \\ M \end{Bmatrix} \quad (2)$$

This stiffness matrix in Eq. (2) represents the soil-pile stiffness at the mudline. Since the matrix is non-diagonal, lateral deformation and rocking modes have coupled spring stiffnesses, which comprise the elements in the stiffness matrix. To obtain these spring constants for the different sea states, the values L and EI from Table 2 are substituted into Eq. (2). Note that these values of L and EI are derived by considering movement only in the x-z plane (lateral deflection in the fore-aft or x direction and rocking in the plane). The same coupled spring stiffnesses that are derived for motion in the x-z plane are applied to the model for motion in the y-z plane as well. Effectively, the same spring stiffnesses are applied for sway and roll degrees of freedom of the structure as those for the surge and pitch degrees of freedom. Thus, we have:

$$\begin{bmatrix} \frac{12EI}{L^3} & 0 & 0 & 0 & -\frac{6EI}{L^2} & 0 \\ 0 & \frac{12EI}{L^3} & 0 & \frac{6EI}{L^2} & 0 & 0 \\ 0 & 0 & 0 & 0 & 0 & 0 \\ 0 & \frac{6EI}{L^2} & 0 & \frac{4EI}{L} & 0 & 0 \\ -\frac{6EI}{L^2} & 0 & 0 & 0 & \frac{4EI}{L} & 0 \\ 0 & 0 & 0 & 0 & 0 & 0 \end{bmatrix} \begin{Bmatrix} surge \\ sway \\ heave \\ roll \\ pitch \\ yaw \end{Bmatrix} = \begin{Bmatrix} TwrBsFxt \\ TwrBsFyt \\ TwrBsFzt \\ TwrBsMxt \\ TwrBsMyt \\ TwrBsMzt \end{Bmatrix} \quad (3)$$

Equation (3) is the overall platform stiffness matrix at the mudline that can be assembled using Eq. (2). Note that sway and heave are coupled to each other in a similar manner to the way surge and pitch are; also, the associated stiffness coefficients are the same except for some sign changes necessary due to the reference sign convention adopted. In Eq. (3), the heave and yaw degrees of freedom are shown only for the sake of completeness; they are not modeled in the foundation flexibility. The vector on the right-hand side of Eq. (3) is comprised of tower base forces and moments in the x, y, and z directions. The total mass of the 36-meter foundation is added as a lumped mass at the mudline to ensure that the CS model has the same total mass as the original structure.

C. Distributed Springs Model

The distributed springs (DS) model replaces the soil surrounding the pile foundation with discrete springs distributed along the length of the pile. The stiffnesses of these springs depend on the shear and moment pair at the head of the pile, and since only one load pair (i.e., F-M pair) will be used to calibrate the DS model, it is important that it is selected so as to be representative of the sea state to which this DS model will be calibrated. Accordingly, the midpoints of the 25 F-M bins, as described in the AF model, weighted according to their relative likelihoods, provide a single F-M pair that was used to represent the sea state. Once these representative pile head loads were selected, the associated soil behavior was then analyzed. The load-deformation behavior of the soil-pile system is nonlinear; the stiffness of the soil under a given load and at a specific depth can be determined from available p-y

curves (or load-deflection curves). Each depth has its own associated *p-y* curve; LPILE was used to analyze the pile for the selected soil profile. The pile head loads (shear and moment) were applied statically. LPILE then computed the distributed resistance and deflection at 252 points along the length of the embedded pile. The local stiffness associated with each point was taken to be the distributed resistance divided by the deflection and multiplied by the tributary length associated with that point. To limit the number of springs employed in the DS model, the discrete local stiffnesses were condensed down to 37 in number, arranged at a one-meter spacing along the length of the pile; of the original 252 stiffnesses, those that fell within the tributary length of a discrete spring were added together. The same discrete spring stiffnesses that were derived for motions in the horizontal *x*-direction were applied to the model in the horizontal *y*-direction as well.

NUMERICAL STUDIES

After stochastic simulations of the offshore wind turbine response are performed, the fore-aft tower bending moment at the mudline is compared for the four foundation models in the two selected sea states. Statistics averaged over 150 simulations are summarized in Tables 3 and 4 for mean wind speeds of 12 m/s and 22 m/s, respectively. Extreme values are of most interest when determining characteristic loads for design; the extreme value of interest here is the global maximum in a single ten-minute simulated load time series. Averages of the 150 ten-minute extreme values are included in the "Max" column of Tables 3 and 4. This maximum value is related to other statistics in the tables as follows:

$$\text{Max} = \text{Mean} + \text{Std. Dev.} \times \text{PF} \tag{4}$$

where this ten-minute extreme is defined to occur PF standard deviations above the mean. Note that PF is also commonly referred to as a "peak factor" on the ten-minute extreme of a random process.

By studying the statistics in Tables 3 and 4, we can gain an understanding of the tower bending moment process. We first compare load statistics between the two sea states; then, we compare load statistics among the four foundation models.

Between the two sea states, the mean fore-aft tower bending moment at the mudline decreases by about 50% when we go from the smaller mean wind speed (12 m/s) and associated significant wave height (6.2 m) to the larger mean wind speed (22 m/s) and associated significant wave height (9.0 m). A decrease in mean load is expected based on the wind turbine's control system. The turbine increases power output as the wind speed increases up to the rated wind speed (around 11.5 m/s); beyond the rated wind speed, the turbine maintains constant power output. If the wind speed continues to increase to levels above the rated wind speed, the blades can pitch alleviating some of the load experienced by the structure of the wind turbine. Constant power is maintained despite the blades pitching because the wind speed is higher. Larger mean loads result for the V = 12 m/s mean wind speed which is near the rated wind speed; mean loads decrease for higher wind speeds. The standard deviation of the tower load is seen to increase with increase in V and H_s. With increasing input energy from the wind and waves, the variance (and, thus, the standard deviation) of the load process is expected to increase—for instance, the tower bending moment standard deviation increases from 17.7 to 18.6 MN-m for the FB model when going from the lower V-H_s sea state to the higher one; similar increases are seen with the flexible foundation models.

The peak factor (PF) on the ten-minute extreme load is seen to also increase though very slightly for the sea state with the larger V and H_s. The peak factor is directly related to exposure time, to the asymmetry and tail behavior of the load distribution, and to the mean upcrossing rate of the load process. The exposure time of ten minutes is the same for both sea states. The asymmetry of the load distributions (represented by the coefficient of skewness values) appear to be not so important because these skewness coefficients are close to zero. If any observation is to be made, it is that with the FB model, the load distribution becomes positively skewed for the sea state with the larger V and H_s which might favor larger PF values; the exact opposite is true for all the flexible foundation models. The kurtosis estimates (which characterize the tail behavior of the load distribution) are slightly larger in Table 4 with the larger V and H_s indicating heavier probability mass in the tails. The mean upcrossing rates of the load process are also higher in Table 4, with largest increases over Table 3 for the FB model. Overall, for the sea state with V = 22 m/s and H_s = 9.0 m, the ten-minute extreme peak factor increased very slightly for the flexible foundation models but more significantly for the FB model. In summary, we see that the large decrease in the mean load, even though it is somewhat offset by an increase in standard deviation and an increase in peak factor (albeit only very slightly for the flexible foundation models), leads to somewhat larger ten-minute maxima for the sea state with V = 12 m/s and H_s = 6.2 m. Based on Eq. (4), we might conclude that the maximum load decreases for the sea state with the higher wind speed and wave height because the change in the mean load (a decrease) is larger than the opposite change (an increase) in the product of the standard deviation and the peak factor.

Next, we consider how the different foundation models affect load statistics for a given sea state. Upon reviewing Tables 3 and 4 separately for each sea state, we see that the three flexible foundation models experience very similar loads as might be expected. These models are calibrated to have the same mass and nearly the same mudline stiffness; hence, the three flexible foundation models have nearly the same first and second tower natural frequencies (in the fore-aft and side-to-side directions) as can be confirmed from Table 5. The response for all the models is simulated with the same wind and wave input time series and the same control system characteristics for a selected sea state. Therefore, the fore-aft tower bending moment process is very similar for the three flexible foundation models. The stiffer (FB) model experiences both lower mean loads as well as lower standard deviations than any

of the flexible foundation models. As the overall system gets more flexible (which is the case for the AF, CS, and DS models), it has lower natural frequencies; these lower frequencies are excited by the low-frequency turbulence and wave input energy. This can be confirmed by studying power spectra of the hub-height longitudinal wind velocity and the sea surface elevation in Fig. 4 for both sea states. Due to the increased low-frequency energy experienced by the flexible foundation models, there is greater variation in loads experienced and thus in standard deviation estimates for those models. Overall, the three flexible foundation models experience higher extreme loads than the FB model does because of their larger mean and larger standard deviation values.

Table 3: Averaged statistics of the fore-aft tower bending moment at the mudline from 150 ten-minute simulations when V = 12 m/s and H_s = 6.2 m.

Model	Max	Mean	Std. Dev.	PF (on max)	Skewness	Kurtosis	Upcrossing Rate
	(MN-m)	(MN-m)	(MN-m)	-	-	-	(s^{-1})
FB	117.1	58.0	17.7	3.3	0.00	2.92	0.14
AF	135.6	64.6	21.6	3.3	0.04	2.90	0.20
CS	136.5	64.6	21.8	3.3	0.04	2.91	0.18
DS	135.1	64.6	21.2	3.3	0.04	2.90	0.22

Table 4: Averaged statistics of the fore-aft tower bending moment at the mudline from 150 ten-minute simulations when V = 22 m/s and H_s = 9.0 m.

Model	Max	Mean	Std. Dev.	PF (on max)	Skewness	Kurtosis	Upcrossing Rate
	(MN-m)	(MN-m)	(MN-m)	-	-	-	(s^{-1})
FB	104.1	34.1	18.6	3.8	0.04	3.27	0.29
AF	113.6	34.5	23.6	3.4	-0.06	3.10	0.22
CS	114.1	34.5	23.8	3.3	-0.07	3.11	0.24
DS	112.2	34.5	22.7	3.4	-0.07	3.13	0.24

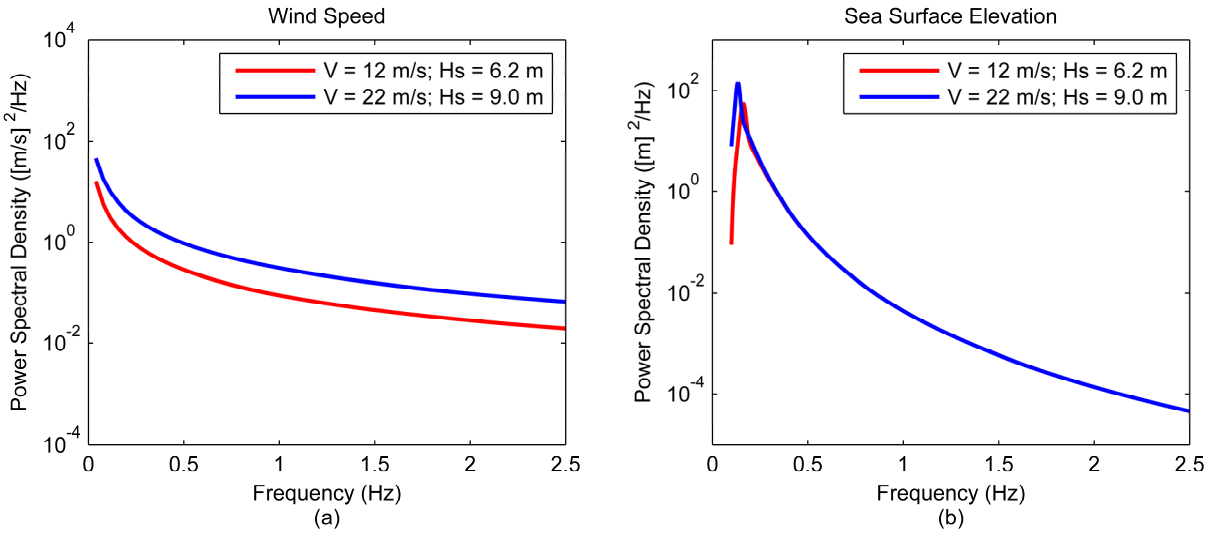

Figure 4: Power spectra of (a) the hub-height longitudinal wind velocity; and (b) the sea surface elevation (for the two sea states considered).

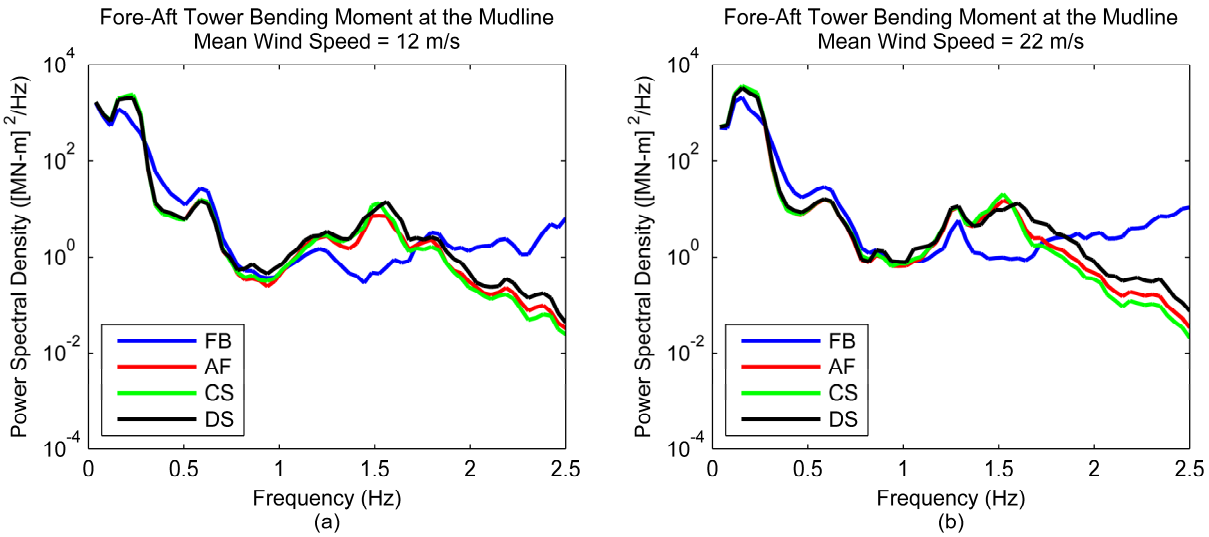

Figure 5: Power spectra of the fore-aft tower bending moment at the mudline for (a) V = 12 m/s; H_s = 6.2 m and (b) V = 22 m/s; H_s = 9.0 m.

Table 5: Natural frequencies of the various foundation models for the two sea states considered.

Model		Natural Frequencies (Hz)			
		1st Tower Fore-Aft	1st Tower Side-to-Side	2nd Tower Fore-Aft	2nd Tower Side-to-Side
FB	-	0.28	0.27	1.83	1.93
AF	V = 12 m/s	0.24	0.24	1.52	1.71
	V = 22 m/s	0.24	0.24	1.50	1.67
CS	V = 12 m/s	0.24	0.24	1.51	1.67
	V = 22 m/s	0.24	0.24	1.49	1.63
DS	V = 12 m/s	0.25	0.25	1.53	1.77
	V = 22 m/s	0.25	0.25	1.53	1.77

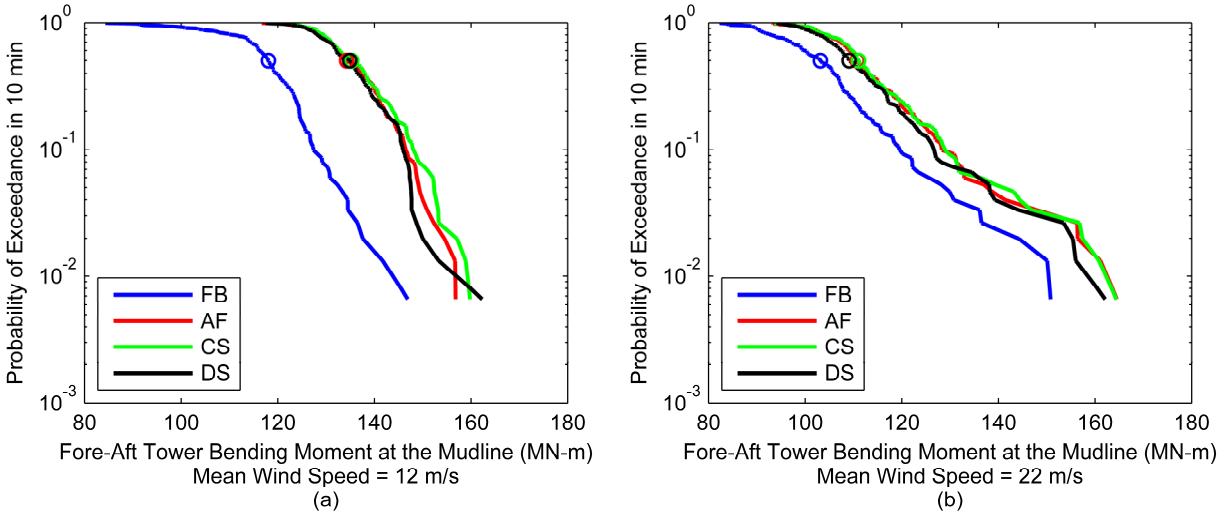

Figure 6: Probability of exceedance plots of the ten-minute extreme fore-aft tower bending moment at the mudline for (a) V = 12 m/s; H_s = 6.2 m and (b) V = 22 m/s; H_s = 9.0 m.

Next, we consider power spectra of the fore-aft tower bending moment at the mudline for the two sea states in Fig. 5. In general, there is little difference between the two sea states. As seen in Table 5, the three flexible foundation models have very similar first natural frequencies and show small differences in second natural frequencies; hence, for a given sea state, the power spectra for the flexible foundation models show only slight differences as well. The FB model is stiffer and, expectedly, its tower bending moment power spectra show greater high-frequency energy.

Finally, in Fig. 6, we consider probability of load exceedance plots for the two sea states. When comparing these two sea states, we see greater variation (overall spread) in ten-minute extreme tower bending moment estimates from 150 simulations for the V = 22 m/s and H_s = 9.0 m sea state. For the V = 12 m/s and H_s = 6.2 m sea state, the load distribution curves are steeper suggesting less load variation in ten-minute extremes. The circles indicated toward the top of the curves identify median ten-minute extreme load estimates; these values are presented in Table 6 as well. When using the environmental contour method (i.e., 2D Inverse FORM), the largest median ten-minute extreme among all sea states on the environmental contour associated with a 20-year return period is selected as the 20-year characteristic load for design. Though a careful inspection of all sea states around this 20-year contour has not been performed, the V = 12 m/s and H_s = 6.2 m sea state is believed to yield an accurate characteristic load based on our study of seven different critical sea states. Hence, the first row in Table 6 shows 20-year characteristic loads for the four foundation models. These four derived characteristic loads were confirmed to have 90% confidence intervals smaller than 5 MN-m based on bootstrap resamplings of the simulated extremes. With such small confidence intervals, it can be concluded that 150 simulations are sufficient to define 20-year characteristic loads with the 2D Inverse FORM approach. A more accurate 3D Inverse FORM approach which accounts for full variability in the tower load extreme (given wind speed and wave height) will require accurate load extreme estimates with lower exceedance probability levels. To achieve tight confidence intervals at those levels, a greater number of simulations will likely be needed as is evident from the tails of the load distribution curves in Fig. 6. Among the flexible foundation models, median ten-minute extreme loads (and, thus, the 20-year characteristic loads) are seen to differ by less than 1% for both sea states studied.

Table 6: Median estimates of the ten-minute extreme fore-aft tower bending moment (for two sea states).

V (m/s)	Median 10-min. Extreme (MN-m)			
	FB	AF	CS	DS
12	118.1	134.3	135.3	134.9
22	103.2	110.8	111.1	109.1

A NOTE ON THE FLEXIBLE FOUNDATION MODELS

In the AF model, the derived stiffness of the foundation is based on *F-M* pairs originating from simulations with the FB model. In reality, these mudline loads are not what the real structure will experience when the flexible foundation model is introduced later. For instance, after running turbine response simulations with the "calibrated" AF model, more accurate mudline *F-M* pairs are available. To assess the accuracy of the AF model procedure that was presented, new mudline loads from the AF model simulations for the V = 12 m/s sea state were used in place of the original FB model mudline loads and recalibration using LPILE of a new AF model was undertaken. The apparent fixity length changed from 16.21 m to 16.03 m. Fifteen simulations were run with both the first- and second-round AF models, and statistics of the fore-aft tower bending moment at the mudline were studied. The global ten-minute maximum, the mean, and the standard deviation all changed by less than one percent. This finding leads us to believe that an iterative fine-tuning step of recalibrating the AF model (as well as other flexible foundation models since they all rely on FB model mudline forces in a similar manner) is unnecessary. We note, however, that this result may not apply in general for any other soil profile or wind turbine than the one considered here.

CONCLUSIONS

Long-term tower loads based on four foundation models have been compared for a shallow-water offshore wind turbine. With any choice of foundation model, ten-minute extreme fore-aft tower bending moments were largest for sea states whose mean load levels were largest; this occurred for a sea state with a mean hub-height wind speed close to the rated wind speed and not for one with a significantly higher mean wind speed. For a given sea state, we see that use of a fixed-base model leads to smaller estimates of standard deviations and extremes of tower bending loads; these estimates are larger when flexible foundation models are employed. Overall, we see that the three flexible models (from a 2D Inverse FORM perspective) are effectively interchangeable because they produce 20-year characteristic loads within 1% of each other. In summary, the significant underestimation of long-term offshore wind turbine loads by fixed-base models compared to flexible foundation models suggests that calibration of flexible foundation models as presented here, based on information from soil profiles, can be helpful in the design of offshore wind turbines with monopile foundations.

ACKNOWLEDGMENTS

The authors are pleased to acknowledge the financial support received from the National Science Foundation by way of two grants—Award Nos. CMMI-0049128 (CAREER) and CMMI-0727989. They thank Dr. Jason Jonkman at the National Renewable Energy Laboratory (NREL) for his continued assistance with the program, FAST, and for the 5 MW wind turbine model used in this study. They thank Ensoft, Inc. for providing LPILE for their use and Dr. Shin Tower Wang, in particular, for his assistance with that program.

Finally, they thank Dr. Puneet Agarwal, a former student at the University of Texas at Austin, for his contributions to this study.

REFERENCES

[1] Passon, P., "Memorandum: Derivation and Description of the Soil-Pile-Interaction Models" IEA-Annex XXIIII Subtask 2, Stuttgart, Germany, 2006.

[2] Jonkman, J., Butterfield, S., Passon, P., Larsen, T., Cap, T., Nichols, J., Azcona, J., and Martinez, A., "Offshore Code Comparison Collaboration within IEA Wind Annex XXIII: Phase II Results Regarding Monopile Foundation Modeling," Proceedings of the IEA European Offshore Wind Conference, Berlin, Germany, 2007.

[3] Jonkman, J. M., Butterfield, S., Musial, W., and Scott, G., "Definition of a 5MW Reference Wind Turbine for Offshore System Development," Tech. Rep. NREL/TP-500-38060, National Renewable Energy Laboratory, Golden, CO, (to be published), 2007.

[4] Winterstein, S. R., Ude, T. C., Cornell, C. A., Bjerager, P., and Haver, S., "Environmental Contours for Extreme Response: Inverse FORM with Omission Factors," Proc. ICOSSAR-93, Innsbruck, 1993.

[5] Chakrabarti, S. K., "Hydrodynamics of Offshore Structures," Springer-Verlag, Berlin, 1987.

[6] International Electrotechnical Commission, "IEC 61400-1: Wind Turbines – Part 1: Design Requirements," Edition 3, 2005.

[7] Jonkman, B. J. and Buhl, M. L. Jr, "TurbSim User's Guide," NREL/TP- 500-41136, National Renewable Energy Laboratory, Golden, Colorado, 2007.

[8] DNV-OS-J101, "Design of Offshore Wind Turbine Structures," Offshore Standard, Det Norske Veritas, 2007.

[9] Jonkman, J. M. and Buhl, M. L. Jr, "FAST User's Guide," National Renewable Energy Laboratory, NREL/EL-500-38230, Golden, CO, 2005.

[10] Reese, L. C., Wang, S. T., Isenhower, W. M., Arréllaga, J. A., and Hendrix, J., 2004, "Computer Program LPILE Plus Version 5.0 User's Guide: A Program for the Analysis of Piles and Drilled Shafts Under Lateral Loads," Ensoft, Inc., Austin, TX.

[11] API RP 2A-WSD, 2000, "Recommended Practice for Planning, Designing and Constructing Fixed Offshore Platforms—Working Stress Design," 21st Edition.